40th Fluid Dynamics Conference and Exhibit
28 June - 1 July 2010, Chicago, Illinois

AIAA 2010-4997

High-order shock-fitting methods for hypersonic flow with chemical and thermal nonequilibrium

Akshay Prakash[1], Neal Parsons[2], Xiaowen Wang[3], and Xiaolin Zhong[4]
University of California, Los Angeles

Computer simulations have been an effective tool to study transient flow processes in hypersonic flow and have been complementing experimental and theoretical studies to better understand the flow transition process. There have been lots of efforts in code development for high order simulation of nonequilibrium flow but most of the methods are based on shock capturing ideodology. Shock capturing schemes may not capture the flow processes with enough accuracy required to study flow transition. The essential requirements of such simulations are high order of accuracy of solutions in both space and time. We have developed a high order shock fitting code capable of simulating thermal and chemical nonequilibrium hypersonic flows. Shock fitting approach has the advantage of capturing the entire flow field with high order accuracy and without any oscillations near the shock which shock capturing schemes may exhibit for strong shocks. We have tested and validated the code thoroughly over a wide span of free stream conditions and geometries. We have implemented the current updated models available in literature for nonequilibrium and transport phenomenon. This code would be starting point for simulations to study real gas effects on receptivity for free stream disturbances and their transition to turbulence in the boundary layer, and for study of transition in ablative boundary layers. Here we present the methodology and validation cases for the code. The code in current form is up to third order accurate in time and fifth order accurate in space.

Nomenclature

δ_{ij}	=	kronecker delta function
μ	=	viscosity
ρ	=	density
τ	=	stress tensor
ν_{es}	=	collision frequency of species s with electron
Ω_{ij}	=	collision cross section for ith and jth species
c	=	speed of sound
c_s	=	species mass fraction
c_p	=	specific heat
C_p	=	heat capacity
dt	=	time step
D_s	=	diffusion coefficient of species s
D	=	diffusion coefficient of mixture
$\hat{I}$	=	ionization energy
E	=	total energy
E_v	=	total vibration energy
E_{vs}	=	vibration energy of species s

[1] Graduate student, Mechanical and Aerospace, akshayprakash@gmail.com, Student member
[2] Graduate student, Mechanical and Aerospace, nealparsons@gmail.com, Student member
[3] Post Doctorate, Mechanical and Aerospace, xiaowen@seas.ucla.edu, AIAA member
[4] Professor, Mechanical and Aerospace, xiaolin@seas.ucla.edu, Associate fellow

e = total specific energy
e_v = specific total vibration energy
e_{vs} = specific vibration energy of species s
$e_{el,s}$ = electronic energy of species s
E_e = total electronic energy
F_j = *Jth* component of the inviscid Flux
F^+ = flux split in +ve direction
F^- = flux split in –ve direction
F_{yj} = *Jth* component of the viscous Flux
h_s = enthalpy of species s
h_s^0, $\hat{D}$ = heat of formation of species s
k = translational-rotational thermal conductivity
J = jacobean
k_f = forward rate constant
k_b = backward rate constant
k_{eq} = equilibrium rate constant
k_B = Boltzman constant
k_v = vibrational conductivity
M_s = molecular mass of species s
P,p = pressure
P_i, p_i = partial pressure for species i
$Q_{T\text{-}Tv}$ = Vibration-Translation energy relaxation
R, $\overline{R}$ = universal Gas constant
T = translational-rotational temperature
T_v = vibrational temperature
u_j = velocity in jth direction
v_j = diffusion velocity in jth direction
U = Conservative variables vector
w_i = weights for calculating average velocity
W = source vector
x_i = mole fraction of species i
x,y,z,t = Cartesian coordinates
ξ,η,ζ,τ = transformed coordinates
z_i = P_i / P

I. Introduction

Modeling thermal and chemical nonequilibrium is an essential part of predicting flow field at hypersonic speeds. The high speed causes the temperature behind the shock to rise to values high enough for air to start reacting. Different modes of energy may not come to equilibrium as air crosses the shock. The most popular model for thermal nonequilbrium is the Park's two temperature model in which translational and rotational energy are in equilibrium and vibrational mode is in ground state immediately behind the shock. Electronic energy is assumed to be in ground state throughout. We have also presented results for 11 species Air model which includes ionic species. In Park's two temperature model, forward rate constants for dissociation reactions depend on averaging of translational and vibrational temperatures. Thus the accuracy of prediction of species concentration depends on the accuracy of the temperatures. At high temperatures, ionization occurs and modeling it is essential for accurately predicting temperature distribution. An important aspect of ionization is radiation in the flow field. Radiation emanating from behind the shock is one of the important sources of surface heating in ablation. Also temperature in the boundary layer is very crucial for modeling receptivity and predicting transition. Also the concentration of species in the boundary layer affects surface reactions and transport properties thus affecting the heat transfer to the surface. This in turn affects ablation and surface properties which then affect transition. Thus any analysis based on the hypersonic flow whether it is prediction of transition,

surface ablation or just the surface forces, including thermal and chemical nonequilibrium in simulations in simulations is of utmost importance for accuracy.

Prediction of flow transition in boundary layer has been studied for a long time and is still a very active research area. Due to advancement of computational technology now real gas effects are being considered in simulations. Malik [28] studied boundary layer stability with chemical equilibrium on adiabatic flat plate. Stuckert and Reed [55] studied the effects of equilibrium and non equilibrium chemical reactions on the stability of Mach 25 flow over 10-degree half angel sharp cone. They used shock fitting approach to eliminate spurious oscillations that could adversely affect stability analysis. They include chemical equilibrium and nonequilibrium for their simulations. They found that unlike equilibrium flow in nonequilibrium flow the supersonic modes could not be related in a straight forward manner to the incoming and outgoing amplified solutions in the inviscid region of shock layer. Another effect of chemical reactions was to increase the size of supersonic region by reducing temperature of the flow field and thus reducing the speed of sound. Johnson et. al. [18] compare equilibrium and nonequilibrium simulations to experimental results. They could reproduce the general trend of increasing transition Reynolds number with decreasing dissociation energies but over predicted the transition Reynolds number by a factor of about 2. Hudson et.al. [17] compared the effects of chemical equilibrium, nonequilibrium and frozen flow on transition and found that nonequilibrium does not affect the transition Reynolds number for their test cases. Ma and Zhong [25] studied the receptivity of free stream disturbances of a Mach 10 nonequilibrium oxygen flow over a flat plate. They also used shock fitting approach to avoid oscillations and get high order of accuracy for their simulations. They found that the real gas effects had strong influence on second mode receptivity of reacting oxygen flow to free stream acoustic waves. They also found that unstable region for nonequilibrium flow in larger than the perfect gas flow implying the effects are destabilizing for the descrete modes in the region. Stemmer et.al. [53, 54] have developed a hybrid code which treats shocks locally through a hybrid ENO method and other areas are dealt with compact finite difference schemes [22]. The authors simulated a flight case along the descent path of the space shuttle at a local Mach number of M=20 and H=50 km and found good agreement with LST [27]. The reacting flow was modeled using 5 species Park model [Park, C., 89-1740]. MacLean et.al. [29] used STABL code to compare simulations with Mach 10 flow over a 7-degree sharp and blunt cone and over a axisymmetric compression surface. The mean flow was obtained using DPLR code. Authors could better predict the transition location on the test cases. This would help further in designing experiments to understand transition better. Leyva et. al. [23] used injection of CO2 in hypervelocity boundary layers to delay transition. The experimental data was obtained from Caltech's T5 reflected shock tunnel and the computations were made using DPLR (for cases without injection) and using a hybrid Unstructured Implicit solver [36]. The simulation results corroborated the experiments and would be used in prediction of injection schemes for new experimental cases.

Effect of surface phenomenon on transition has been a subject of study since the study of ablation. It was recognized very early that during reentry the transition to turbulence increased the heat transfer to the surface and the increased the amount of material ablated. It is important to optimize the amount of ablative material to maximize the payload. A large number of researchers have modeled ablation in terms of surface reactions such as oxidation and nitridation, sublimation and surface gas injection. To understand ablation better it is very crucial that we understand how transition is affected by surface phenomenon.
Some of recent works include Cabrit et.al [4] studied effects of ablation on turbulent boundary layer thorough DNS. They modeled ablation through pyrolysis, sublimation and surface reactions. DNS was performed using AVBP. AVBP is a finite element code based on TTGC scheme (Taylor Galerkin 3rd order scheme) with temporal integration through multistage RK methods. They modeled surface reactions through two heterogeneous reactions involving solid carbon, CO2 and H2O. They found that for their particular case effect of wall ablation was not predominant.

Current state of the art codes modeling nonequilibrium processes include US3D [36], LAURA [11, 12] and DPLR [61, 62]. DPLR (Data Parallel Line Relaxation) from NASA Ames and LAURA (Langley Aerothermodynamic Upwind Relaxation Algorithm) from NASA Langley are both structured grid finite volume codes capable of doing parallel multiblock simulations with chemical and thermal nonequilibrium in laminar flow fields. DPLR, as the name suggests utilizes data parallel line relaxation method to integrate solutions in time. The inviscid flux is calculated using modified Steger-Warming flux splitting [26] and MUSCL extrapolation to reach third order accuracy in space. Species diffusion

coefficients are calculated using self-consistent effective binary diffusion method [47, 48] and using the Yos [65] and Gupta [13] mixing rules. Species thermodynamic properties are calculated using curve fits of Gordon and McBride [30]. Thermal nonequilibrium is modeled using two temperature Park model [45]. The relaxation model is based on the Landau-Teller formulation with relaxation time being calculated from Milikan and White formulation [31]. Equilibrium constants for chemical source terms are calculated using minimum Gibbs free energy approach [30]. For forward reaction rates different models from Park are used [15].

LAURA utilizes Roe-averaging [49] with Harten's entropy fix [14] and Yee's TVD limiter to obtain inviscid fluxes. Either of point implicit or implicit line integration can be used for time advancement. LAURA is different from DPLR in handling the electronic energy – it assumes electronic energy to be in equilibrium with vibrational energy. LAURA calculates diffusion coefficients based on Schmidt number.

US3D utilizes unstructured grids for discretization. US3D can utilize line relaxation for time integration like DPLR, and has an option of doing a point implicit integration throughout the flow field except in boundary layer where it utilizes the line relaxation method. US3D is different from DPLR in handling the electronic energy – setting it to be in equilibrium with translational-rotational energy modes.

All the three codes compute the viscous fluxes to second order accuracy in space. A more comprehensive neck to neck comparison between the codes was done by Hash et. al.[15]. The authors use FIRE II experiment as the test bed to evaluate the performance of the three codes.

A. Scope of Current Study

We have developed a high order shock fitting code which has been already validated and has been used for study of receptivity and transition analysis of free stream disturbances to the boundary layer flow [676869] for quite some time. Here we extend the code to include real gas models to study their effects on receptivity of free stream disturbances and their transition in boundary layer. For studying transition we need to have high order accuracy in space and time. Shock capturing methodology has the disadvantage of reducing to first order near the shock. Also it produces artificial oscillations near the shock which is not desirable in studying transition. We use shock fitting approach with finite difference discretization scheme from Zhong [67] to achieve high order accuracy in space and SIRK schemes from Zhong [64] to achieve high order accuracy in time integration. The code has 5 species reaction without ionization and electronic excitation and 11 species ionized Air model with electronic excitation. Thermal nonequilibrium is modeled using two temperature model of Park [45]. For chemical source terms the code has Parks 1985 [41] and 1990 [38], Gordon-McBrides model [30] for equilibrium constants, Park's updated model [38] for reaction rates. Thermal nonequilibrium is modeled using Landau Teller formulation with thermal relaxation time given by Milikan's data [31]. Transport coefficients are modeled using self consistent effective binary diffusion coefficients by Ramshaw [47, 48] and Blottners curve fits for species viscosity. Properties for mixture are evaluated using Yos [65] mixing rule and Wilke's mixing rule [59]. We rigorously tested the code and present some validation results. The test cases are Mach 15 case and Mach 7 case of Lobb [24], Double cone case from Roy [350]. Mach 15 case from Lobb is essentially a reacting test case. The maximum temperature rise in the flow field is about 12000K. So this case would test the nonequilibrium implementation of the code. Mach 7 case is comparatively lower temperature case and the solution is not much different from ideal gas simulation. Both the Lobb's cases are relatively low Re number cases. Double Cone test cases by Candler are shock interaction computations and experiments over flared double cone. Test run by Holden were done to study the effect of thermal nonequilibrium in the free stream. We cannot simulate shock shock interaction with the current code as it is. So we would compute the relevant part of the geometry where the flow in not effected by the interaction and compare our results with published data. Also test cases with thermal nonequilibrium in the free stream are rarified gas flows and need slip conditions on the boundary to predict the flow field correctly. We run a test case by Roy [50] which was used to compare DSMC results with Navier-Stokes code. The case is a nitrogen gas flow over double cone flare. We have also developed 11 species code with ionization model. A true test for such a code would be high mach number flow like FIRE II. For the current paper we compare Lobb's Mach 15 case on this model. The temperatures in this case are not large enough for ionization. However the predictions for the 11 species code match well with the 5 species code and shock standoff compares well with the published data.

The code will be used to study transition with real gas effects. As mentioned earlier, transition in not fully understood and not much has been done to understand the effect of real gas. We plan to study the receptivity of free stream disturbances with real gas models and also the effects of surface reactions on flow transition.

B. The Physical Process

Hypersonic flow over blunt body is characterized by complex non equilibrium phenomenon. Due high temperature rise just behind the shock, there is a non equilibrium region in which air composition is different from its equilibrium value and it starts reacting. If the temperature is too high the thermal modes of energy also get excited and depending on the Reynolds number of the flow, take some distance to come to equilibrium. If the temperature goes sufficiently high, ionization may occur – which may result in radiation. Also for reentry flows it has been observed that a significant amount of surface heating is due to the radiation that originates just behind the shock. Due to high temperature in the flow field, surface phenomena start which includes catalysis, pyrolysis, surface degradation through sublimation and spallation. Surface degradation leaves a rough surface which may assist in early transition, change the shape and weight structure of the vehicle resulting in an entirely different force field. It is very important to accurately predict the flow variables to predict heat transfer rates, transition location and body forces accurately. Modeling all these complex phenomena is further exacerbated by the unreliability of transport and reaction data at high temperatures.

II. Methodology

A. Governing Equations

The governing equations are essentially the Navier Stokes equations. They are split into viscous, inviscid and source terms. The first five equations are species continuity equations. Next three equations are momentum equation in the three coordinates. Then there is the governing equation for energy and finally the governing equation for vibrational energy. Here we assume that the three diatomic molecules (and the 8 diatomic molecules for 11 species code) are in thermal equilibrium and have the same vibrational temperature which is in equilibrium with electronic temperature for the 11 species code.

$$\frac{\partial U}{\partial t}+\frac{\partial F_j}{\partial x_j}+\frac{\partial F_{vj}}{\partial x_j}=w \tag{2.1}$$

$$U=\begin{bmatrix}\rho_{N_2}\\ \rho_{O_2}\\ \rho_{NO}\\ \rho_N\\ \rho_O\\ \rho u_1\\ \rho u_2\\ \rho u_3\\ E_v\\ E\end{bmatrix}\quad F_j=\begin{bmatrix}\rho_{N_2}u_j\\ \rho_{O_2}u_j\\ \rho_{NO}u_j\\ \rho_N u_j\\ \rho_O u_j\\ \rho u_1 u_j+p\delta_{1j}\\ \rho u_2 u_j+p\delta_{2j}\\ \rho u_3 u_j+p\delta_{3j}\\ E_v u_j\\ (E+p)u_j\end{bmatrix}\quad F_{vj}=\begin{bmatrix}\rho_{N_2}v_{N_2 j}\\ \rho_{O_2}v_{O_2 j}\\ \rho_{NO}v_{NOj}\\ \rho_N v_{Nj}\\ \rho_O v_{Oj}\\ \tau_{j1}\\ \tau_{j2}\\ \tau_{j2}\\ k_v\frac{\partial T_v}{\partial x_j}+\sum_s \rho e_{vs}D\frac{\partial c_s}{\partial x_j}\\ \tau_{ji}u_j+k\frac{\partial T}{\partial x_j}+k_v\frac{\partial T_v}{\partial x_j}+\sum_s \rho_s h_s v_{sj}\end{bmatrix}\quad W=\begin{bmatrix}w_{N_2}\\ w_{O_2}\\ w_{NO}\\ w_N\\ w_O\\ 0\\ 0\\ 0\\ Q_{T-v}+\sum_s w_s e_{vs}\\ 0\end{bmatrix} \tag{2.2}$$

$$\tau_{ij} = \mu\left(\frac{\partial u_i}{\partial x_j} + \frac{\partial u_j}{\partial x_i}\right) - \frac{2}{3}\mu\frac{\partial u_k}{\partial x_k}\delta_{ij} \tag{2.3}$$

Here μ is the viscosity coefficient determined by the Sutherland law:

$$\mu = \mu_r\left(\frac{T}{T_r}\right)^{\frac{3}{2}}\frac{T_r + T_s}{T + T_s} \tag{2.4}$$

This is used for ideal gas flows. For multispecies model we have the Bolttner's curve fit data for viscosity and the viscosity for mixture is evaluated using Wilke's mixing rule. Transport coefficients based on collision cross-section data are also implemented and have been described later.

The species u_{sj} velocity can be written as [1]:

$$u_{sj} = v_{sj} + u \tag{2.5}$$

Note that 'j' denotes the coordinate variable and 's' denotes the specie, v_{sj} is the diffusion velocity calculated using the Ficks law:

$$\begin{aligned} \rho_s v_{sj} &= \rho D_s \frac{\partial c_s}{\partial x_j} \\ c_s &= \rho_s / \rho \\ Le &= \frac{D\rho c_p}{k} \end{aligned} \tag{2.6}$$

Here D_s is the species diffusion coefficient calculated based on Lewis number which is assumed to be constant for all species. Diffusion coefficients based on collision cross section data have also been implemented based on Gupta's report [13]:

$$D_{ij} = \frac{kT}{\Delta_{ij}^{(1)}} \tag{2.7}$$

The thermal diffusion coefficient for a species in a mixture can then be calculated by:

$$D_i^T = \left(1 - \frac{w_i}{w}\right)\left(\sum_{i \neq j}\frac{z_j}{D_{ij}}\right)^{-1} \tag{2.8}$$

Here $w_i = x_i = z_i$ for single temperature systems.

As mentioned in the equations above, the average velocity is then grouped with the inviscid terms and solved using local Lax Friedrich Flux splitting, while the diffusion velocity is grouped with the viscous terms. The source terms due to chemical reactions and vibrational relaxation are put separately in 'w'. These equations are transformed into body fitted curvilinear coordinates:

$$\begin{cases} \xi = \xi(x,y,z) \\ \eta = \eta(x,y,z) \\ \varsigma = \varsigma(x,y,z) \\ \tau = t \end{cases} \Leftrightarrow \begin{cases} x = x(\xi,\eta,\varsigma,\tau) \\ y = y(\xi,\eta,\varsigma,\tau) \\ z = z(\xi,\eta,\varsigma,\tau) \\ t = \tau \end{cases} \tag{2.9}$$

$$\frac{1}{J}\frac{\partial U}{\partial \tau} + \frac{\partial E'}{\partial \xi} + \frac{\partial F'}{\partial \eta} + \frac{\partial G'}{\partial \varsigma} + \frac{\partial E'_v}{\partial \xi} + \frac{\partial F'_v}{\partial \eta} + \frac{\partial G'_v}{\partial \varsigma} + U\frac{\partial\left(\frac{1}{J}\right)}{\partial \tau} = w$$

A fifth-order (third-order) explicit finite difference scheme [67] is used for spatial discretization of the governing equations, the inviscid flux terms are discretized by the upwind scheme, and the viscous flux terms are discretized by the central high order scheme. For the inviscid flux vectors, the flux Jacobeans contain both positive and negative eigenvalues, a simple local Lax-Friedrichs scheme is used to split vectors into negative and positive wave fields. For example, the flux term F′ can be split into two terms of pure positive and negative eigenvalues as follows:

$$\begin{aligned} F' &= F'_+ + F'_- \\ F'_\pm &= \frac{1}{2}\left(F' \pm \lambda U\right) \end{aligned} \tag{2.10}$$

λ is chosen to be larger than the local maximum of eigenvalues of F′:

$$\begin{aligned} \lambda &= \frac{|\nabla \eta|}{J}\left(\sqrt{(\varepsilon c)^2 + u'^2} + c\right) \\ u' &= \frac{\eta_x u + \eta_y v + \eta_z w}{|\nabla \eta|} \end{aligned} \tag{2.11}$$

The parameter ε is a small positive constant added to adjust the smoothness of the splitting. The fluxes F'_+ and F'_- contain only positive and negative eigenvalues respectively. Therefore, in the spatial discretization of the differential equation, the derivative of the flux F is split into two terms:

$$\frac{\partial F'}{\partial \eta} = \frac{\partial F'_+}{\partial \eta} + \frac{\partial F'_-}{\partial \eta} \tag{2.12}$$

The first term on the right hand side is discretized by the upwind scheme and the second term by the downwind scheme. The fifth-order explicit (third-order) scheme utilizes a 7-point (5-point) stencil and has an adjustable parameter α as follows [67]:

$$u'_i = \frac{1}{hb_i}\sum_{k=-3}^{3}\alpha_{i+k}u_{i+k} - \frac{\alpha}{6!b_i}\left(\frac{\partial u^6}{\partial^6 x}\right)_i + \cdots \tag{2.13}$$

The scheme is upwind where $\alpha < 0$ and downwind when $\alpha > 0$. It becomes a six-order central scheme when $\alpha = 0$.

B. Shock Fitting

The solution procedure is base on shock fitting by Zhong [67]. The domain between the shock and blunt body is discretized and solved based on the Local Lax Friedrich flux splitting. The conditions behind the shock are calculated using the Rankine Hugoniot relations:

$$\left(\bar{F}_s - \bar{F}_\infty\right) \bullet l_s + \left(U_s - U_\infty\right) l_t = 0$$
$$l_s = \left(\frac{\eta_x}{J}\right)\hat{i} + \left(\frac{\eta_y}{J}\right)\hat{j} + \left(\frac{\eta_z}{J}\right)\hat{k} \tag{2.14}$$
$$l_t = \frac{\eta_t}{J}$$

The shock may be moving and its velocity (and the grid velocity) is calculated by differentiating the above expression in time and using the following compatibility relationships:

$$\vec{l}_{N-1} \bullet \left[\frac{\partial\left(U/J\right)}{\partial\tau} + \frac{\partial F_1^{'}}{\partial\xi} + \frac{\partial F_2^{'}}{\partial\eta} + \frac{\partial F_3^{'}}{\partial\zeta} - w\right] = 0$$
$$\vec{l}_{N-1} \bullet A_s^{'} = \frac{|\nabla\eta|}{J}\left(u^{'} + c\right)\vec{l}_{N-1} \tag{2.15}$$

$$\vec{l}_{N-1} = \begin{bmatrix} \frac{\gamma-1}{2}\left(\mathbf{u}.\mathbf{u} - h_1^0\right) - cu_n \\ \frac{\gamma-1}{2}\left(\mathbf{u}.\mathbf{u} - h_i^0\right) - cu_n \\ \frac{\gamma-1}{2}\left(\mathbf{u}.\mathbf{u} - h_{NS}^0\right) - cu_n \\ -\left(\frac{1}{2}cn_x - \frac{\gamma-1}{2}u\right) \\ -\left(\frac{1}{2}cn_y - \frac{\gamma-1}{2}v\right) \\ -\left(\frac{1}{2}cn_z - \frac{\gamma-1}{2}w\right) \\ \frac{\gamma-1}{2} \\ -\frac{\gamma-1}{2} \end{bmatrix} \tag{2.16}$$

The equations are discretized (inviscid terms by 5th (3rd) order finite difference scheme and viscous terms by 6th (4th) order central difference schemes) and solved in time using Runge Kutta methods.

C. Chemical Reaction

We have considered 5 species presently with the following reactions [2]:

$$N_2 + M \Leftrightarrow N + N + M$$
$$O_2 + M \Leftrightarrow O + O + M$$
$$NO + M \Leftrightarrow N + O + M \tag{2.17}$$
$$N_2 + O \Leftrightarrow NO + N$$
$$NO + O \Leftrightarrow O_2 + N$$

The reaction rates can be written as:

$$
\begin{aligned}
R_1 &= \sum_s \left[-k_{f1s} \frac{\rho_{N2}}{M_{N2}} \frac{\rho_M}{M_M} + k_{b1m} \frac{\rho_N}{M_N} \frac{\rho_N}{M_N} \frac{\rho_M}{M_M} \right] \\
R_2 &= \sum_s \left[-k_{f2s} \frac{\rho_{O2}}{M_{O2}} \frac{\rho_M}{M_M} + k_{b2m} \frac{\rho_O}{M_O} \frac{\rho_O}{M_O} \frac{\rho_M}{M_M} \right] \\
R_3 &= \sum_s \left[-k_{f3s} \frac{\rho_{NO}}{M_{NO}} \frac{\rho_M}{M_M} + k_{b3m} \frac{\rho_N}{M_N} \frac{\rho_O}{M_O} \frac{\rho_M}{M_M} \right] \\
R_4 &= -k_{f4} \frac{\rho_{N2}}{M_{N2}} \frac{\rho_O}{M_O} + k_{b4} \frac{\rho_{NO}}{M_{NO}} \frac{\rho_N}{M_N} \\
R_5 &= -k_{f5} \frac{\rho_{NO}}{M_{NO}} \frac{\rho_O}{M_O} + k_{b5} \frac{\rho_{O2}}{M_{O2}} \frac{\rho_N}{M_N}
\end{aligned}
\tag{2.18}
$$

And hence the species source terms are:

$$
\begin{aligned}
w_{N2} &= M_{N2} \left(R_1 + R_4 \right) \\
w_{O2} &= M_{O2} \left(R_2 + R_5 \right) \\
w_{NO} &= M_{NO} \left(R_3 - R_4 + R_5 \right) \\
w_N &= M_N \left(-2R_1 - R_3 - R_4 - R_5 \right) \\
w_O &= M_O \left(-2R_2 - R_3 + R_4 + R_5 \right)
\end{aligned}
\tag{2.19}
$$

The reaction rates were calculated using the following relations [41]:

$$
\begin{aligned}
&K_f = C_f \bar{T}^{\eta} \exp\left(-\theta / \bar{T} \right) \quad \bar{T} = \sqrt{T\, T_v} \\
&K_b = K_f / K_{eqr} \\
&K_{eqr} = A_{0r} \exp\left(\frac{A_{1m}}{z} + A_{2m} + A_{3m} \ln(z) + A_{4m} z + A_{5m} z^2 \right) \quad z = 10000 / T
\end{aligned}
\tag{2.20}
$$

The values of reaction constants are given reference [41, 19, 38]. Note that the forward reaction rates for dissociation reactions would be at a temperature that is the geometric mean of vibrational and translational temperature. The backward reaction rates and forward reaction rates for exchange reaction would depend on translational-rotational temperature alone.

The source terms involving chemical reactions may become stiff, i.e. the rates for some reactions maybe orders of magnitude higher than the others. To overcome this we use point implicit scheme for reacting source terms. For case of a well stirred reactor, backward Euler can be written as:

$$
\left(I - \Delta t \left[\frac{\partial W}{\partial U} \right]^{n+1} \right) \Delta U^{n+1} = W^n - \Delta U^n \tag{2.21}
$$

Here $\partial W / \partial U$ is the Jacobean of the source term w. Other high order integration methods are the SIRK (Semi Implicit Runge Kutta methods) by Zhong [64]. We have implemented third order SIRK schemes for high order integration in time. The integration is done in point implicit fashion and would help overcome any stiffness in the source terms.

$$
\frac{dU}{dt} = F_{ns}(U) + F_s(U) \tag{2.22}
$$

$$
\begin{aligned}
&[I - a_1 \Delta t J(U^n)]k_1 = \Delta t[F_{ns}(U^n) + F_s(U^n)] \\
&[I - a_2 \Delta t J(U^n)]k_2 = \Delta t[F_{ns}(U^n + b_{21}k_1) + F_s(U^n + c_{21}k_1)] \\
&[I - a_3 \Delta t J(U^n)]k_3 = \Delta t[F_{ns}(U^n + b_{31}k_1 + b_{32}k_2) + F_s(U^n + c_{31}k_1 + c_{32}k_2)] \\
&U^{n+1} = U^n + \omega_1 k_1 + \omega_2 k_2 + \omega_3 k_3
\end{aligned}
\tag{2.23}
$$

Another reaction model- 11 species Air ionization model has been implemented. It consists of the following dissociation reactions:

$$
\begin{aligned}
&N_2 + M \Leftrightarrow N + N + M \\
&O_2 + M \Leftrightarrow O + O + M \\
&NO + M \Leftrightarrow N + O + M
\end{aligned}
\tag{2.24}
$$

, the following exchange reactions:

$$
\begin{aligned}
&N_2 + O \Leftrightarrow NO + N \\
&NO + O \Leftrightarrow O_2 + N
\end{aligned}
\tag{2.25}
$$

, the follwing ion exchange reactions:

$$
\begin{aligned}
&O^+ + N_2 \Leftrightarrow N_2^+ + O \\
&O^+ + NO \Leftrightarrow N^+ + O_2 \\
&NO^+ + O_2 \Leftrightarrow O_2^+ + NO \\
&NO^+ + N \Leftrightarrow N_2^+ + O \\
&NO^+ + O \Leftrightarrow N^+ + O_2 \\
&O_2^+ + N \Leftrightarrow N^+ + O_2 \\
&O_2^+ + N_2 \Leftrightarrow N_2^+ + O_2 \\
&NO^+ + N \Leftrightarrow O^+ + N_2 \\
&NO^+ + O \Leftrightarrow O_2^+ + N
\end{aligned}
\tag{2.26}
$$

, the following ionization reactions:

$$
\begin{aligned}
&N + O \Leftrightarrow NO^+ + e^- \\
&N + N \Leftrightarrow N_2^+ + e^- \\
&O + O \Leftrightarrow O_2^+ + e^-
\end{aligned}
\tag{2.27}
$$

, the following electron assisted ionization reactions:

$$
\begin{aligned}
&N + e^- \Leftrightarrow N^+ + e^- + e^- \\
&O + e^- \Leftrightarrow O^+ + e^- + e^-
\end{aligned}
\tag{2.28}
$$

And the following electron assisted dissociation:

$$
N_2 + e^- \Leftrightarrow N + N + e^- \tag{2.29}
$$

Like the 5 species model reactions rates and source terms for each of the 11 species can be written based on these reactions. For the first three reactions, the forward rate constants are based on the average of

vibration and translation temperature and backward and equilibrium rates are based on translation temperature only. For the second (exchange) and third group (ion exchange) reactions, both forward and backward reactions are based on translation temperature. For the fourth group forward reactions are based on translation temperature while backward reactions are based on vibration temperature. For the fifth (electron assisted ionization) group and the last reaction (electron assisted dissociation) both forward and backward reaction rates are based on vibration temperature.

The reaction rates were computed using the following curve fits:

$$\begin{aligned} K_f &= C_f \bar{T}^{\eta} \exp\left(-\theta \big/ \bar{T}\right) \quad \bar{T} = \sqrt{T\, T_v} \\ K_b &= K_f \big/ K_{eqr} \\ K_{eqr} &= A_{0r} \exp\left(\frac{A_{1m}}{z} + A_{2m} + A_{3m} \ln(z) + A_{4m} z + A_{5m} z^2\right) \quad z = 10000/T \end{aligned} \tag{2.30}$$

The values for the constants were taken from dissertation of Scalabrin [52]. The reaction constants are those listed for DPLR code.

D. Vibrational Energy

The equation for vibration energy is solved in similar way to energy equation. The vibration energy is defined as [19, 44, 1]:

$$E_{vs} = \sum \frac{\rho_s R_s \theta_{vs}}{e^{\theta_{vs}/T_v} - 1} \tag{2.31}$$

However there is only one overall vibration energy equation. It is solved and the vibration temperature is calculated using Newton's method. Also note that unlike the energy term there is a source term which consists of vibration energy from translational energy and due to formation of diatomic species.

Also note that the total energy term includes vibration energy and chemical energy terms. The total energy can be written as:

$$E = \sum_s C_{vs} T + \frac{1}{2} \rho u_i u_i + \sum_s E_{vs} + \sum_s \rho_s h_s^0 \tag{2.32}$$

The exchange between vibration and translation energy can be calculated using [31, 42, 43, 44, and 46]:

$$Q_{TV} = \sum_s \rho_s \frac{e_{vs}(T) - e_{vs}(T_v)}{\langle \tau_{s-LT} \rangle + \tau_{cs}} \tag{2.33}$$

Where $\tau_{s\,LT}$ is the Landau Teller vibration relaxation given by [21, and 31]:

$$
\begin{aligned}
\left\langle \tau_{s-LT} \right\rangle &= \frac{\sum_r x_r}{\sum_r x_r / \tau_{sr-LT}} \\
\tau_{sr-LT} &= \frac{1}{p}\exp\left[A_{sr}\left(T^{-1/3} - 0.015\mu_{sr}^{1/4} \right) - 18.42 \right], \text{ p in atm} \\
A_{sr} &= 1.16\times 10^{-3}\,\mu_{sr}^{1/2}\theta_{vs}^{4/3} \\
\mu_{sr} &= \frac{M_s M_r}{M_s + M_r}
\end{aligned}
\tag{2.34}
$$

Where,

$$
\begin{aligned}
\tau_{cs} &= \frac{1}{c_s \sigma_v N_s} \\
c_s &= \sqrt{8RT/\pi M_s} \\
\sigma_v &= 10^{21}\left(50000/T \right)^2
\end{aligned}
\tag{2.35}
$$

E. Electronic energy

The electronic energy for the species was modeled using the following reaction:

$$
e_{el,s} = \begin{cases} \dfrac{R_u}{M_s}\dfrac{\sum_{i=1}^{\infty} g_{i,s}\theta_{el,i,s}\exp\left(-\theta_{el,i,s}/T_{ve}\right)}{\sum_{i=0}^{\infty} g_{i,s}\exp\left(-\theta_{el,i,s}/T_{ve}\right)} & \text{for molecules and atoms} \\ 0 & \text{for electrons} \end{cases}
\tag{2.36}
$$

Here T_{ve} is taken as the vibration temperature which we assume to be in equilibrium with the electronic temperature. The constants are taken from dissertation of Scalabrin [52]. Electronic excitation is implemented in the 11 species air model only. For this model the electronic and vibration energy is combined into a single equation [11]:

$$
\begin{aligned}
&\frac{\partial}{\partial t}\rho e_V + \frac{\partial}{\partial x^j}\rho e_V u^j = -p_e\frac{\partial u^j}{\partial x^j} + \frac{\partial}{\partial x^j}\left[\left(\eta_v + \eta_e \right)\frac{\partial T_V}{\partial x^j} \right] + \frac{\partial}{\partial x^j}\left(\rho\sum_{s=1}^{11} h_{V,s} D_s \frac{\partial c_s}{\partial x^j} \right) + \\
&\sum_{molecules} \rho_s \frac{\left(e_{v,s}^* - e_{v,s} \right)}{\left\langle \tau_s \right\rangle} + 2\rho_e \frac{3}{2}\overline{R}\left(T - T_V \right)\sum_{s=1}^{10}\frac{\upsilon_{es}}{M_s} - \sum_{ionized}\dot{n}_{e,s}\hat{I}_s + \sum_{ionized}\dot{w}_s\hat{D}_s
\end{aligned}
\tag{2.37}
$$

Here $e_V = e_v + e_e$, represents the combined vibration and electronic energy. Electron pressure is computed in the same manner as translational rotational pressure. Term 5 on the right hand side is energy exchange model between electrons and molecules and atoms. υ_{es} is the collision frequency and is computed as follows[11]:

$$\upsilon_{es} = \frac{8}{3}\left(\frac{\pi}{m_e}\right)^{1/2} n_s e^4 \frac{1}{\left(2kT_e\right)^{3/2}} \ln\left(\frac{k^3 T_e^3}{\pi n_e e^6}\right) \qquad \text{for charged species}$$
$$\upsilon_{es} = n_s \sigma_{es} \left(\frac{8kT_e}{\pi m_e}\right)^{1/2} \qquad \text{for neutral species} \tag{2.38}$$

Here σ_{es} is the collision cross section area and the values used are from dissertation of Scalabrin [52]. The sixth term on the right side is the loss in electronic energy due to electron induced ionizations. The relevant species are the ions and $\dot{n}_{es}$ is the rate of production of species s expressed in kg per cubic meter, $\hat{I}_s$ is the first ionization energy of species s expressed in joules per mole. There are two reactions when ionization occurs due to electron impact. The constants for these terms have been taken from dissertation of Scalabrin [52]. Terms 2 and 3 on right hand side are computed along with diffusion terms. First term on right along with others is treated as source term.

F. Viscosity and Heat conductivity

The viscosity and heat conductivity of gas mixture is modeled by Blottner's curve fits and by Gupta's mixing rule [13], where species viscosities and heat conductivities are calculated using non-columbic collision cross section data [13]. This model is valid for higher speed flows, on the order of 10 km/s. Using Blottner's data, viscosity and translational conductivity of gas mixture is obtained according to the following formulae [1]:

$$\mu_s = 0.1 \exp\left[\left(V_A \log T + V_B\right)\log T + V_C\right] \tag{2.39}$$

The mixture transport properties are calculated using Wilke's mixing rule [59]:

$$\mu = \sum_s \frac{x_s \mu_s}{\phi_s}, \quad k = \sum_s \frac{x_s k_s}{\phi_s}$$
$$x_s = \frac{c_s}{M_s \sum_s c_s / M_s} \tag{2.40}$$
$$\phi_s = \sum_r x_r \left[1 + \sqrt{\frac{\mu_s}{\mu_r}}\left(\frac{M_r}{M_s}\right)^{1/4}\right]^2 \left[\sqrt{8\left(1+\frac{M_s}{M_r}\right)}\right]^{-1}$$

Transport coefficients were calculated from cross section data following Gupta's methods [13] by the following equations:

$$\mu \text{ or } K_{tr} = \frac{\sum_{s=1}^{5} x_i / \left(A_i + a_{av}\right)}{1 - a_{av} \sum_{i=1}^{NS} x_i / \left(A_i + a_{av}\right)}$$
$$a_{av} = \frac{\sum_{i,j=1}^{NS} x_i x_j \left(\frac{1}{A_i} - \frac{1}{A_j}\right)^2 a_{ij}}{\sum_{i,j=1}^{NS} x_i x_j \left(\frac{1}{A_i} - \frac{1}{A_j}\right)^2} \tag{2.41}$$
$$A_i = \sum_{l=1}^{NS} x_l B_{il}$$

For thermal conductivity, a_{ij} and B_{ij} are defined as:

$$\begin{aligned} a_{ij} &= \left(\frac{2}{15k}\right)\frac{2M_iM_j}{\left(M_i+M_j\right)^2}\left[\left(\frac{33}{2}-\frac{18}{5}B_{ij}^*\right)\Delta_{ij}^{(1)}-4\Delta_{ij}^{(2)}\right] \\ B_{il} &= \left(\frac{2}{15k}\right)\frac{1}{\left(M_i+M_j\right)^2}\left[8M_iM_l\Delta_{il}^{(2)}+\left(M_i-M_l\right)\left(9M_i-\frac{15}{2}M_l+\frac{18}{5}B_{il}^*M_l\right)\Delta_{il}^{(1)}\right] \end{aligned} \tag{2.42}$$

For viscosity, a_{ij} and B_{ij} are defined as:

$$\begin{aligned} a_{ij} &= \frac{N_A}{\left(M_i+M_j\right)}\left[2\Delta_{ij}^{(1)}-\Delta_{ij}^{(2)}\right] \\ B_{il} &= \frac{N_A}{M_i}\Delta_{il}^{(2)} \end{aligned} \tag{2.43}$$

Quantities $\Delta_{ij}^{(1)}, \Delta_{ij}^{(2)}$ are defined as:

$$\begin{aligned} \Delta_{ij}^{(1)} &= \frac{8}{3}\left[\frac{2M_iM_j}{\pi R_{univ}T\left(M_i+M_j\right)}\right]^{1/2}\pi\bar{\Omega}_{i,j}^{(1,1)} \\ \Delta_{ij}^{(2)} &= \frac{16}{5}\left[\frac{2M_iM_j}{\pi R_{univ}T\left(M_i+M_j\right)}\right]^{1/2}\pi\bar{\Omega}_{i,j}^{(1,1)} \end{aligned} \tag{2.44}$$

The collision cross sections are defined as:

$$\begin{aligned} \pi\bar{\Omega}_{i,j}^{(1,1)} &= \left[\exp\left(D_{\bar{\Omega}_{ij}^{(1,1)}}\right)\right]T^{\left[A_{\bar{\Omega}_{ij}^{(1,1)}}\left(\ln T\right)^2+B_{\bar{\Omega}_{ij}^{(1,1)}}\ln T+C_{\bar{\Omega}_{ij}^{(1,1)}}\right]} \\ \pi\bar{\Omega}_{i,j}^{(2,2)} &= \left[\exp\left(D_{\bar{\Omega}_{ij}^{(2,2)}}\right)\right]T^{\left[A_{\bar{\Omega}_{ij}^{(2,2)}}\left(\ln T\right)^2+B_{\bar{\Omega}_{ij}^{(2,2)}}\ln T+C_{\bar{\Omega}_{ij}^{(2,2)}}\right]} \\ B_{ij}^* &= \left[\exp\left(C_{B_{ij}^*}\right)\right]T^{\left[A_{B_{ij}^*}\ln(T)+B_{B_{ij}^*}\right]} \end{aligned} \tag{2.45}$$

Conductivity for vibration temperature and rotational excitation (which is added to translational conductivity) is computed via the following formula:

$$K_V \text{ or } K_{rot} = k\sum_{i=1}^{NS}\frac{\frac{C_{P,v \text{ or } rot}}{R_{univ}}x_i}{\sum_{j=1}^{NS}x_j\Delta_{ij}^{(1)}} \tag{2.46}$$

In equations above, k is the Boltzmann constant, and R is gas constant. K_t, K_r, K_V are heat conductivity components relating to translational energy, rotational energy, and vibration energy (including electronic energy), respectively. In current paper, values of A, B, C, and D in equation above are obtained

from a more recent paper of Hash et al. [15], where the parameters are correlated from the new data recommended by Wright et al. [60].

III. Validation Results

The tests were computed using two different models for 5 species code and with 11 species code. 5 species code consists of non ionic species in air - N_2, O_2, NO, N, O. The reaction constants are from Park 1990 [25]. When computing the diffusion terms for species transport, we use Blottner's model [1] as Model 1and computation of transport properties using collision cross section data and species diffusion terms via Ramshaw's self consistent binary diffusion model [47, 48] as Model 2. 11 species code consists of ionic species - $N_2, O_2, NO, N_2^+, O_2^+, NO^+, N, O, N^+, O^+, e^-$. This model is appropriate for high temperature cases when ionization in significant. This model also takes into account the electronic excitation of molecules which the 5 species model ignores. This model uses Blottner's curve fits for viscosity and Wilke's mixing rule to calculate mixture transport properties. Diffusion coefficients are based on constant Lewis number.

A. Lobb's (1964) experiment:

The experiment consists of firing spheres of 0.5 in diameters into air at mach 15.3. The Reynolds number for this flow is 26480. The ambient conditions are defined by T_∞ = 293 K and ρ_∞ = 7.83E-3 kg/m^3. Free stream is air and we take the mass fractions to be N_2 = 0.79 and O_2 = 0.21.

This test case has a Mach number high enough for thermal and chemical non equilibrium to exist. We get very good agreement for shock standoff distance with Lobb's experimental results and Candler's simulations as shown in figure 1. The shock standoff distance matches exactly at the stagnation point and compares well away from it. The computations from Model 1 , Model 2 and 11 species code are shown in the figure. All the three computations agree well on shock standoff distance. Figure 2 shows stagnation line temperature variation. Line with symbols is Candler's computations. Solid lines are computations with Model 1 and dashed with Model 2. Both Models predict same temperature profiles. Slight variation can be seen near the shock where temperatures are very high. Both models agree very well with Candler's computations near the surface. As in the figure, immediately after the shock, the translation-rotation temperature rises to about 11000K, but the vibration temperature still remains at its free stream value. As the flow progresses, vibration and translation temperature close down and near the surface are almost equal. The temperature in the flow field is roughly around 6000K. At this temperature oxygen is almost completely dissociated while a significant portion of nitrogen should be dissociated. Candler's computations were made using three different vibration temperatures for each diatomic species and electron. The vibration temperature shown in the figure for Candler's computations is that for Nitrogen. Since there is almost no ionization for this temperature range (as in evident in the results of 11 species code) the differences with Candler's computations are due to different model of vibration energy.

Figure 3 compares the stagnation line temperature for the three different Models used. Model 1 and Model 2 compare well. However the 11 species code predicts different values through the flow field except near the surface where all the three models agree very well. The difference is due to the electronic energy excitation for species with 11 species model takes into account. Note that there is little ionization at this temperature in the flow field. Electronic energy is modeled with the vibration energy. So for the 11 species code electronic excitation is additional degree of freedom which lowers the vibration temperature slightly, which in turn lowers the average value of translation and vibration temperatures. This causes the species to dissociate less – as in evident in Figure 6, and hence slightly higher value of predicted translation temperature.

Figure 4 compares species mass fraction along stagnation line with Candler's computations. The average temperature of Candler is lower for nitrogen and hence we expect lesser dissociation for nitrogen. However that is not clear from the figure because shock standoff distance is not exactly the same. Candler's

computations were made using shock capturing methodology which smears the shock over some grid points. These computation were made before the Park 1990 model (which we used), hence there is slight difference in shock standoff distance. Although not exact, the trend compares well. Nitrogen and oxygen start dissociating due to high temperatures. Oxygen dissociates completely as expected. Nitrogen also dissociates a little again going back to its free stream value at the wall which is at much lower temperature than the flow field. NO concentration peaks behind the shock and goes back to zero again at the wall. Near the shock, due to low vibration temperature, the average temperature is lower and in the zone where NO is stable and as the vibration temperature rises, NO vanishes. Values for NO concentration differ completely from Candler's computations. Candler's computations show maximum mass fractions to be about 0.1 while we predict it to be slightly lower than 0.2. The general trend and the point of maximum agree with Candler's computations and the discrepancies are due to the different model used.

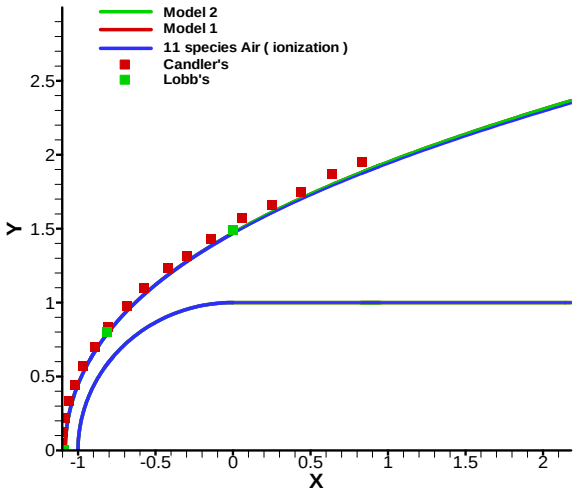

Figure 1. Shock standoff distance: *Comparison with Lobb's experiment and with Candler's computations.*

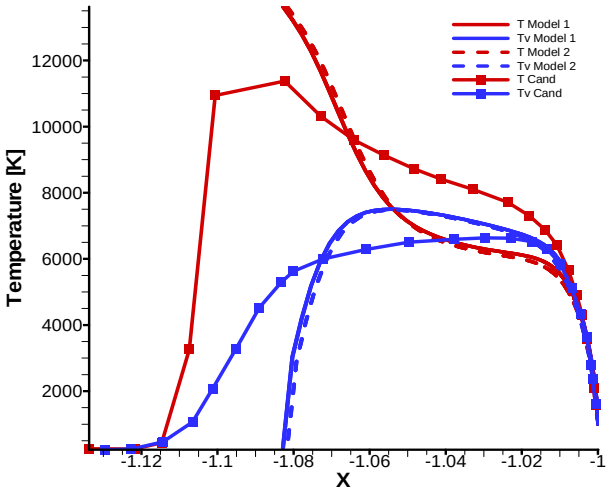

Figure 2. Temperature profile along stagnation line: *Comparison with Candler's computations.*

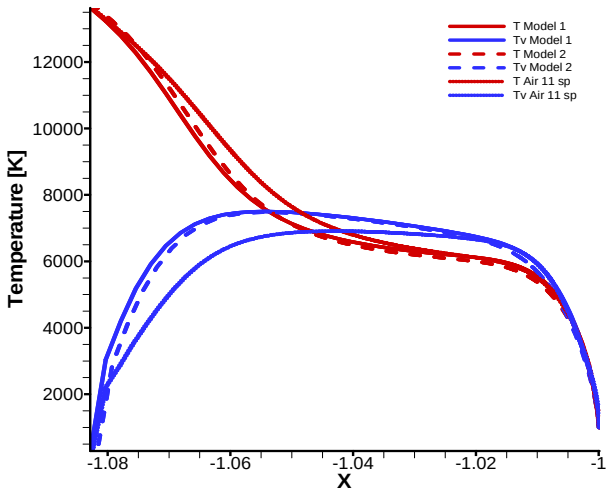

Figure 3. Variation of temperature along stagnation line: *comparison of different Models.*

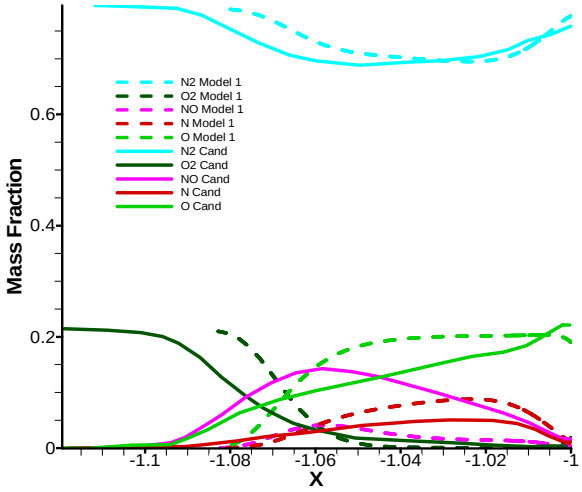

Figure 4. Variation of species mass fraction along stagnation line: *comparison of Model 1 with Candlers computations.*

Figure 5 compares mass fractions for Model 1 and Model 2. There is not much difference both predict almost identical concentrations. However Model 2 is more accurate as it is based on collision cross section data and computes diffusion consistently (ensures that net diffusion is zero). Figure 6 compares mass fractions predicted by 11 species code and that by 5 species code. Species concentration depends strongly on temperature and this figure corroborates that. There was a slight difference in temperature profiles of 11 species code and 5 species code and the effects on species concentration are visible in this figure. Due to smaller average temperature the dissociation of Nitrogen and Oxygen is lesser in the 11 species. Near the wall when temperature is same for all the models, the species concentration seems to converge to same values. Away from the wall when temperatures differ, the concentration of the species differ too. Also note that the 11 species code predicts higher mass fractions of NO than the 5 species. Another point to observe is that the shock standoff distance for both the codes is same. This indicates that the electronic excitation is not large enough to effect the shock standoff and takes only a small fraction of

the total energy. This is also evident in the temperature profiles – there is only a small difference in temperature predicted by the two codes.

Figure 7 compares contours for temperature in the flow field. Although the temperautres predicted by the two codes differ slightly in the stagnation region, in the flowfield they are identical as in figure 7 the contours predicted by Model 1, Model 2 and 11 species code lie on top of each other. This is because the temperature at stagnation was very high causing species dissociation. As in figure 8, distribution of temperautre along the x=0 line, The temperatures are not very high, the tranlation temperature predicted by the three codes is almost the same. Thought the vibration temperature predicted by 11 species code is lower than the 5 species code indicating that there is small amount of electronic excitation.

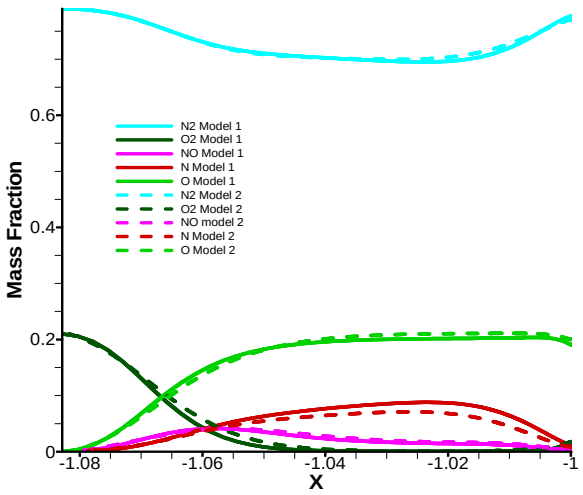

Figure 5. Variation of species mass fraction along stagnation line: *comparison of Model 1 with Model 2.*

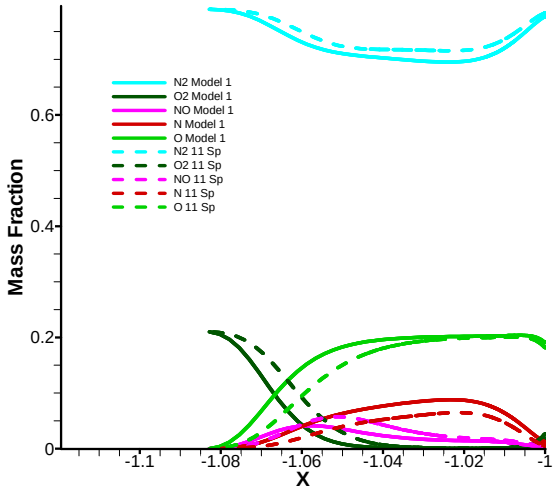

Figure 6. Variation of species mass fraction along stagnation line: *comparison of Model 1 with 11 species code.*

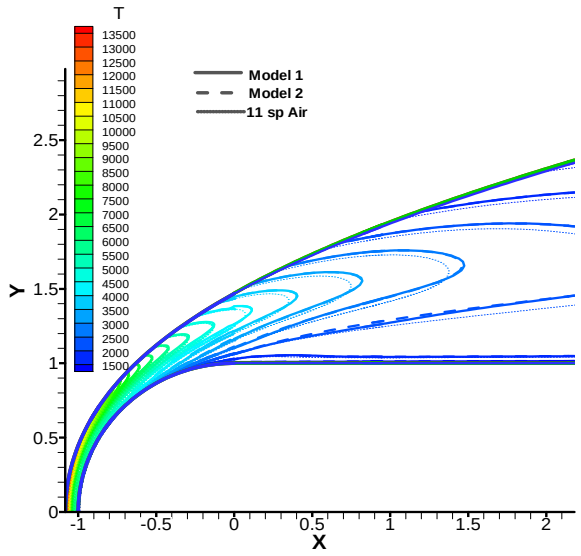

Figure 7: Comparision of Temperature profiles in the flow field.

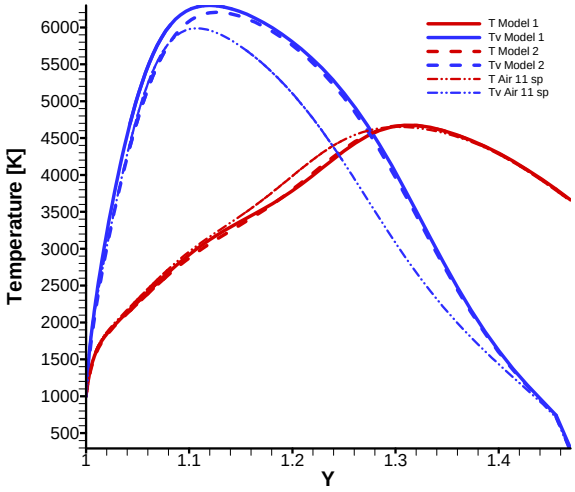

Figure 8: Comparision of Temperature profiles along x=0.

Flow conditions for Mach 7 case:

This experiment consists of firing spheres of 0.5 in diameter into air at mach 7.1. The ambient conditions are defined by T_∞ = 293 K and ρ_∞ = 1.565E-3 kg/m^3. Free stream is air and we take the mass fractions to be N_2 = 0.79 and O_2 = 0.21.

This test case does not have a very high mach number and the flow field is very similar to ideal gas flow field. Here also we get excellent agreement with Candler's simulations. Figure 9 shows shock standoff distance compared with Candler's simulations. We get very good comparison with Candler's results and with Lobb's experimental results. The red squares are Candler's results and the green squares are Lobb's experimental data. Figure 10 compares the translation and vibrational temperature along stagnation line with Candler's computations. The comparison is very good but one must remember that the vibration energy is solved differently than Candler's. Like previous case we compare our common vibration temperature with Candler's computation of vibration temperature of Nitrogen. Since this is

relatively low temperature case, the vibration energy is not excited enough to make translation temperature different for the two models. Note that though the translation temperature matches exactly, the vibration temperature is a little off.

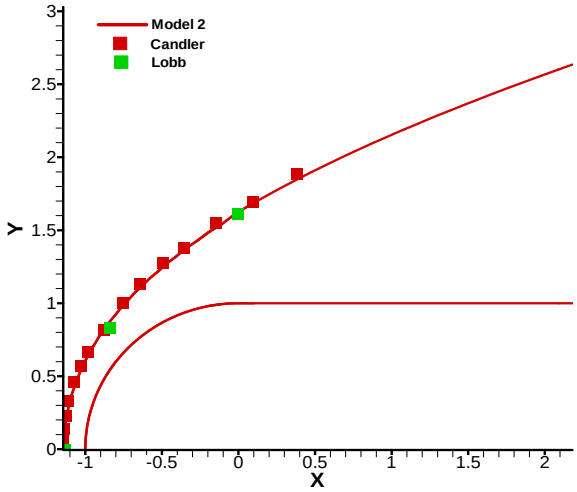

Figure 9. Shock standoff distance matched with Candlers simulations.

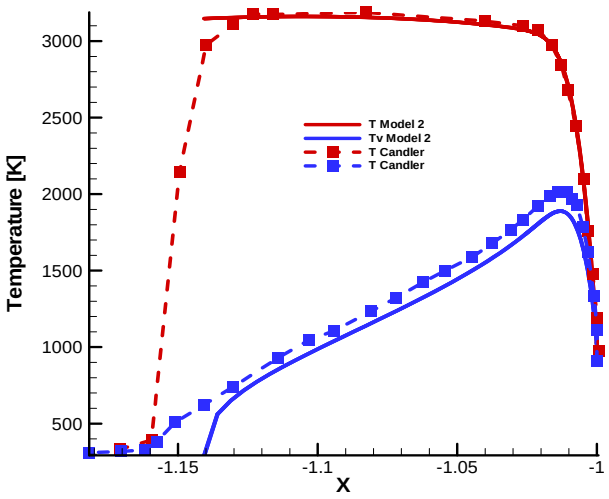

Figure 10. Variation of temperatures along stagnation line compared with Candler's simulations.

B. Double Cone Case:

Double Cone experiments are a series of run over flared cone with blunt and sharp noses to provide validation data for comparison of DSMC and Navier Stokes methods [16, 5051]. The flow conditions are $T_{v\infty}$ = 2772 K and ρ_{∞} = 5.67E-4 kg/m^3, P_{∞}=18.064Pa. Free stream is air. These test cases are in the regime of rarified gas flows and require slip surface boundary conditions. Here we compute a

case computed by Roy earlier [50] on a similar geometry of double cone with flare with free stream such that vibration and translation temperatures are in equilibrium. Also the free stream was purely Nitrogen. The flow conditions are $T_{v\infty}$ = 14.44 K and ρ_{∞} = 5.258E-4 kg/m^3, P_{∞} =21.99Pa. Flared cones have shock-shock interaction which our code cannot model as it is. So we compute the relevant part of the flow field where the flow is laminar without any complicated flow separation or shock-shock interactions. So we compute only the nose and the first cone. The nose radius for this case is 0.25 inch and the cone angle is 25 degrees from horizontal. We do not compute the flare region.

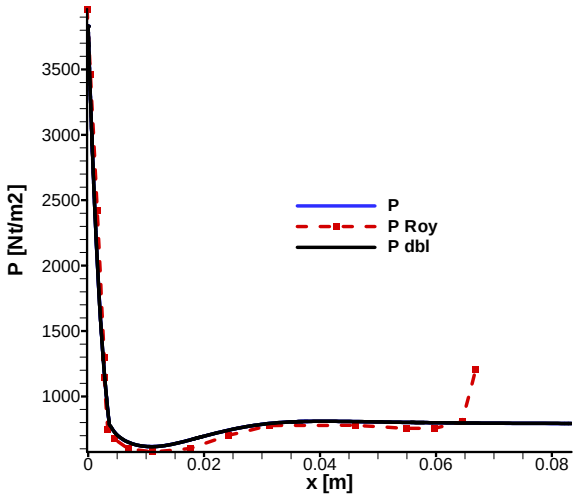

Figure 11. Comparison of Pressure with Roy's computations.

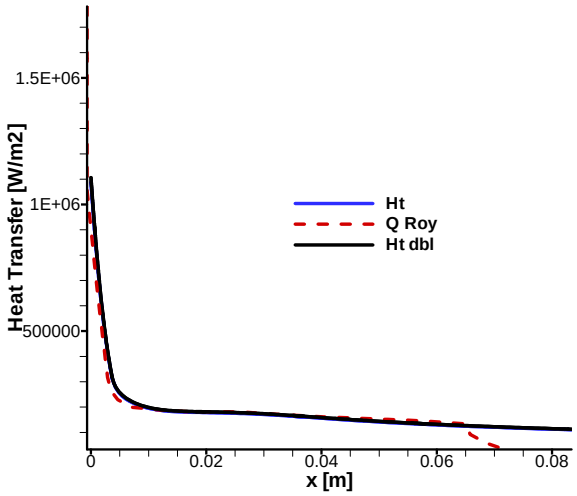

Figure 12. Comparison of heat transfer rates with Roy's computations.

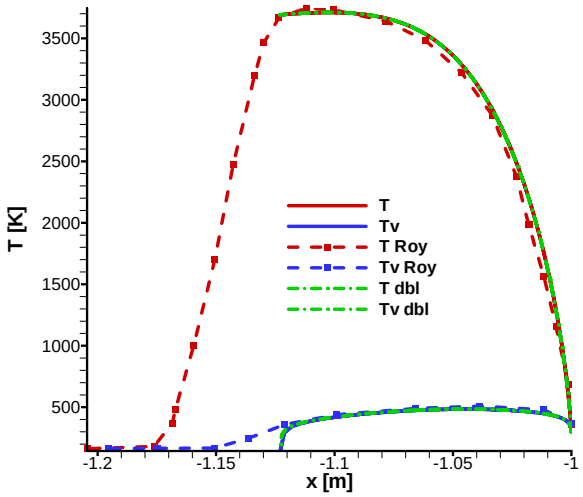

Figure 13. Comparison of heat transfer rates with Roy's computations.

Figure 11 compares surface pressure with computations of Roy [51] and with experimental data. The comparison is very good. Coefficient of pressure is not very sensitive to temperature boundary conditions. At the stagnation region we predict slightly lower value than Roy but over the surface the comparison is excellent. Pressure is highest at the stagnation and drops steadily towards the shoulder region. At the shoulder there is a dip due to change in geometry of the body. Thereafter the pressure is almost constant for us. For Roy's computation the flow encounters the flare region where the pressure starts to rise very sharply. This is the region of flow separation and shock-shock interaction. Figure 12 compares heat transfer rates with those computed by Roy. Here again we have excellent agreement throughout expect at the stagnation and at the beginning of the flare region. Heat transfer is highest at the stagnation and steadily decreases as the flow approaches shoulder. Then it drops of very slowly over the cone region. For Roy's simulations, as the flow encounters the flare zone, there is a sharp drop in heat transfer rate followed by a very sharp increase (not shown here). This is the region of flow separation and shock interaction. Figures 11 and 12 have grid convergence results shown in black lines computed on double grid. Figure 13 compares stagnation temperature profiles with Roy's computations. Again this is not a very high temperature case. The highest temperature reached is about 3700K. There is almost no vibration relaxation. The vibration temperature is about 500 K for most of the flow field. Roy's computations are using shock capturing approach and the smearing of the shock over grid points is evident against the sharp interface of shock fitting approach. DSMC calculations however predict a much larger smeared region.

IV. Future Work

.

We aim to study the receptivity of free stream disturbances for the nonequilibrium flow over blunt bodies and study flow transition in presence of surface chemistry. This code would be a starting point for development of such codes. We need the solutions to be high order accurate in time and space. Flow transition is an active area of research and is not very well understood. Not much has been published about flow transition in non equilibrium or receptivity of free stream disturbances in nonequilibrium flow fields. We need to implement reaction models with carbon species for simulation of surface phenomenon. It would be interesting to see the effects of surface catalysis in addition to surface blowing and suction.

Acknowledgement: The research was supported partially by AFOSR USAF, under AFOSR Grant # FA9550-07-1-0414 monitored by Dr. John Schmisseur and partially by DOE office of Science as part of a SciDAC (Scientific Discovery thorough Advanced Computing) project with "Science Application" in Turbulence. The views and conclusions contained herein are those of the authors and should not be interpreted as necessarily representing the official policies or endorsements either expressed or implied of AFOSR or US Govt.

V. References

1. Blottner, F.G., Johnson, M., and Ellis, M., "Chemically Reacting Viscous Flow Program for Multi-Component Gas Mixtures", Report No. SC-RR-70-754, Sandia Laboratories, Albuquerque, New Mexico.
2. Candler, G.V., "The Computation of weakly ionized hypersonic flows in thermo chemical nonequilibrium", PhD thesis, June, 1988.
3. Candler, G.V., Nompelis, I., Druguet, M.C., Holden, M.S., Wadhams, T.P., Boyd, I., Wang, W.L., "CFD Validation of Hypersonic Flight: Hypersonic Double-Cone Flow Simulations", AIAA 2002-0581.
4. Carbid, O., Artal, L. and Nicoud, F., "Direct Numerical Simulation of Turbulent Multispecies Channel Flow with Wall Ablation", AIAA 2007-4401.
5. Chen, Y.K., Henline, W.D., Chemical nonequilibrium Navier-Stokes solutions for hypersonic flow over an ablating graphite nosetip. AIAA paper 93-2836, 1993.
6. Chen, Y.K., Henline, W.D., Hypersonic nonequilibrium Navier-Stokes solutions over an ablating graphite nosetip. Journal of Spacecraft and Rockets. 1994. 31(5): p. 728-734.
7. Chen, Y.K., Milos, F.S., Navier-Stokes Solutions with Finite Rate Ablation for Planetary Mission Earth Reentries Journal of Spacecraft and Rockets 2005. 42(6):p. 961-970.
8. Chen, Y.K., Milos, F.S., Three-Dimensional Ablation and Thermal Response Simulation Sys. AIAA paper 2005-5064 2005.
9. Conti, R.J., MacCormak, R.W., Groener, L.S., Fryer, J.M., Practical Navier Stokes computation of axis-symmetric reentry flow fields with coupled ablation and shape change AIAA paper 1992-752, 1992:p. 1-9.
10. Curry, D.M., An Analysis of a Charring Ablation Thermal Protection System. NASA TN D-3150, 1965.
11. Gnoffo, P.A., Gupta, R.N., Shinn, J.L., "Conservation Equations and Physical Models for Hypersonic Air Flows in Thermal and Chemical Nonequilibrium", NASA TP-2867, February 1989.
12. Gnoffo, P.A., "An Upwind Biased, Point-Implicit Relaxation Algorithm for Viscous, Compressible Perfect-Gas Flows", NASA TP-2953, 1990.
13. Gupta, R.N., Yos, J. M., Thompson, R. A., and Lee, K-P., *A Review of Reaction Rates and Thermodynamic and Transport Properties for an 11-Species Air Model for Chemical and Thermal Nonequilibrium Calculations to 30 000 K*. 1990, NASA Reference Publication 1232
14. Harten, A., "High Resolution Schemes for Hyperbolic Conservation Laws", JCP, Vol. 49, No. 3, 1983, pp. 357-393.
15. Hash, D., Olejniczak, J, Wright, M. J., Dinish, P., Pulsonetti, M., Hollis, B. R., Gnoffo, P. A., Barnhard, M., Nompelis, I., and Candler, G., *FIRE II Calculations for Hypersonic Nonequilibrium Aerothermodynamics Code Validation: DPLR, LAURA, and US3D*. 2007, AIAA 2007-0605.
16. Holden, M.S., Wadhams, T.P., Harvey, J.K., Candler, G.V., "Comparisons between Measurements in Regions of Laminar Shock Wave Boundary Layer Interaction in Hypersonic Flows with Navier Stokes and DSMC Solutions", RTO-TR-AVT-007-V3.
17. Hudson, M.L., Chokani, N. and Candler, G.V., "Linear Stability of Hypersonic Flow in Thermochemical Nonequilibrium", AIAA Journal, Vol. 35, No. 6, 1997.
18. Johnson, H.B., Trevor, G.S. and Candler, G.V., "Numerical study of hypersonic reacting boundary layer transition on cones", Physics of Fluids, Vol. 10, No. 10, 1998.
19. Kruger, C. H., Vincenti, W. G., "Introduction to Physical Gas Dynamics", John Wiley and Sons, 1965.
20. Kuntz, D.W., Hassan, B., Potter, D.L., Predictions of Ablation Hypersonic Vehicles Using an Iterative Coupled Fluid/Thermal Approach. Journal of Thermophysics and Heat Transfer 2001. 15(2):p.129-139.
21. Lee, J.H., Basic Governing Equations for the Flight Regimes of Aeroassisted Orbital Transfer Vehicles. Thermal Design of Aeroassisted Orbital Transfer Vehicles, ed. H.F. Nelson, Progress in Aeronautics and Astronautics, 96, pp. 3-53, 1985.

22. Lele, S.K., "Compact Finite-Difference Schemes With Spectral-Like Resolution", J. Computational Phys., 104, 16-42, Academic Press, San Diego, 1992.
23. Leyva, I.A., Laurence, S., Beierholm, W., Hornung, H.G., Wagnild, R., Candler, G., "Transition delay in Hypervelocity Boundary Layers by means of CO2/acoustic instability interactions", AIAA 2009-1287.
24. Lobb, R.K., "Experimental Measurement of Shock Detachment Distance on Spheres Fired in Air at Hypervelocities", AD0284378, Naval Ordnance Lab White Oak MD, Dec 1962.
25. Ma, Y. and Zhong, X., "Receptivity to Freestream Disturbances of a Mach 10 Nonequilibrium Reacting Oxygen Flow over a Flat Plate", AIAA 2004-0256.
26. MacCormack, R.W., and Candler, G.V., "The solution of the Navier Stokes Equations Using Gauss-Seidel Line Relaxation", Computers and Fluids, Vol. 17, No. 1, 1989, pp. 135-150.
27. Mack, L.M., "Boundary-Layer Stability Theory", Jet Propulsion Laboratory, Pasadena, USA, JPL Report 900-277 Rev. A, 1969.
28. Malik, M.R., "Predction and Control of Transition in Hypersonic Boundary Layers", AIAA Paper 87-1414
29. MacLean, M., Mundy, E., Wadhams, T., Holden, M., Johnson, H., Candler, G., "Comparisions of Transition Prediction using PSE-Chem to Measurments for a Shock Tunnel Envirunment", AIAA 2007-4490.
30. McBride,B., Zehe, M., Gordon, S., "NASA Glenn Coefficients for Calculating Thermodynamic Properties of Individual Species", Glenn Research Center, Cleveland, OH, NASA TP 2002-211556, (2002).
31. Millikan, R.C., and White, D.R., Systematic of Vibrational Relaxation. J. of Chem. Phys. 39, pp. 3209-3213, 1963.
32. Milos, F.S., Rasky, D.J., Review of numerical procedures for computational surface thermo-chemistry. Journal of Thermophysics and Heat Transfer 1994. 8(1):p. 24-34.
33. Milos, F.S., Chen, Y.K., Comprehensive model for multi-component ablation thermo-chemistry. AIAA paper 1997-141, 1997.
34. Moyer, C. B. R., R. A., An Analysis of The Coupled Chemically Reacting Boundary Layer and Charring Ablator Part II Finite Difference Solution for the In-Depth Response of Charring Materials Considering Surface Chemical and Energy Balances. NASA CR-1061, 1966.
35. Murray, A.L., Russell, G.W., Coupled Aeroheating/Ablation Analysis for Missile Configurations. AIAA paper 2000-2587, 2000.
36. Nompelis, I., Drayna, T., Candler, G.V., "Development of a Hybrid Unstructured Implicit Solver for the Simulation of Reacting Flow over Complex Geometries", AIAA 2004-2227.
37. Park, C., "A Review of Reaction Rates in High Temperature Air, AIAA paper 89-1740.
38. Park, C., "Nonequilibrium Hypersonic Aerothermodynamics", John Wiley and Sons, 1990.
39. Park, C., Review of Chemical-Kinetic Problems of Future NASA Missions, I: Earth Entries, Journal of Thermophysics and Heat Transfer, Vol. 7, No. 3, 1993, pp. 384-398.
40. Park, C., Howe, J.T., Jaffe, R.L., and Candler, G.V., Review of Chemical-Kinetic Problems of Future NASA Missions II: Mars Entries, Journal of Thermodynamics and Heat Transfer, Vol. 8, No. 1, 1994, pp. 9-23.
41. Park, C., On Convergence of Computation of Chemically Reacting Flows. AIAA Paper no. 85-0247, 1985.
42. Park, C., Calculation of Nonequilibrium Radiation in the Flight Regimes of Aeroassisted Orbital Transfer Vehicles, ed. H.F. Nelson, Progress in Aeronautics and Aeronautics, 96, pp. 395-418, 1985.
43. Park, C., Assessment of Two-Temperature Kinetic Model for Dissociating and Weakly ionized Nitrogen. AIAA Paper No. 86-1347, 1986.
44. Park, C., Assessment of Two-Temperature Kinetic Model for Dissociating and Weakly ionizing Air. AIAA Paper No. 87-1574, 1987.
45. Park, C., Assessment of Two-Temperature Kinetic Model of Air", J. of Thermophysics and Heat Transfer, Vol. 3, No. 3, 1989, pp. 233-244.
46. Parker, J.G., Rotational and Vibrational Relaxation in Diatomic Gasses. Physics of Fluids, 2, pp. 449-462, 1959.

47. Ramshaw, J.D., "Self Consistent Effective Binary Diffusion in Multicomponent Gas Mixtures", J. Non-Equilibrium Thermodynamics, Vol 15, 1990, No. 3.
48. Ramshaw, J.D., "Hydrodynamic Theory of Multicomponent Diffusion and Thermal Diffusion in Multitemperature Gas Mixtures", J. Nonequilibrium Thermodynamics, Vol. 18 (1993), pages 121-134.
49. Roe, P.L., "Approximate Riemann Solvers, Parameter Vectors and Difference Schemes", JCP, Vol. 43, No. 2, 1981, pp. 357-372.
50. Roy, C.J., Bartel, T.J., Gallis, M.A., Payne, J.L., "DSMC and Navier-Stokes Predictions for Hypersonic Laminar Interacting Flows", AIAA 2001-1030.
51. Roy, C.J., Gallis, M.A., Bartel, T.J., Payne, J.L., "Navier Stokes and DSMC Simulations for Hypersonic Laminar Shock-Shock Interaction Flows", AIAA 2002-0737.
52. Scalabrin, L.C., "Numerical Simulation of Weakly Ionized Hypersonic Flow over Reentry Capsules", PhD. Dissertation, University of Michigan, 2007.
53. Stemmer, C. and Adams, N.A., "Investigation of Hypersonic Flat-Plate Boundary Layer Transition by direct Numerical Simulation" in High Performance computing in Science and Engineering' 04, Springer 2005.
54. Stemmer, C., "Transition Investigation on Hypersonic Flat-Plate Boundary Layer Flow with Chemical and Thermal Nonequilibrium" in Fluid Mechanics and Its Applications, Springer 2006.
55. Stuckert, G. and Reed, H.L., "Linear Disturbances in Hypersonic, Chemically Reacting Shock Layers", AIAA Journal, Vol. 32, No. 7, July 1994.
56. Suzuki, T.S., Furudate, M., Sawada, K., Unified Calculation of Hypersonic Flow-field for a Reentry Vehicle. Journal of Thermophysics and Heat Transfer. 2002. 16(1): P. 94-100.
57. Wadhams, T.P. and Holden, M.S., "Summary of Experimental Studies for Code Validation in the LENS Facility and Comparisons with Recent Navier-Stokes and DSMC Solutions for Two and Three Dimensional Separated Regions in Hypervelocity Flows", AIAA 2004-917.
58. Wen, Chihyung, "Hypervelocity Flow over Spheres", PhD. Thesis, California Institute of Technology, Pasadena, California, 1994.
59. Wilke, C.R., "A Viscosity Equation for Gas Mixtures", J. of chemical physics, vol. 18, No. 4, 1950.
60. Wright, M.J., Bose, D., Palmer, G. E., and Levin, E., *Recommended collision integrals for transport property computations, part I: air species.* AIAA Journal, 2005. 43(12): p. 2558-2564
61. Wright, M.J., Candler, G.V., Bose,D., "Data-Parallel Line Relaxation Method for the Navier-Stokes Equations", AIAA Journal, Vol. 36, No. 9, Nov. 1998, pp 1603-1609.
62. Wright, M.J., Loomis, M.A., Papadopoulos, P.E., "Aerothermal Analysis of the project FIRE II Afterbody Flow", J. of Thermophysics and Heat Transfer, Vol. 17, No. 2, 2003, pp. 240-249.
63. Yee, H.C., Implicit and Symmetric Shock Capturing Schemes, NASA TM-89464, May 1987.
64. Zhong, X., "Additive Semi-Implicit Runge-Kutta Methods For Computing High Speed Nonequilibrium Reacting flows", JCP, 128, 19-31 (1996).
65. Yos, J.M., "Transport Properties of Nitrogen, Hydrogen, Oxygen, and Air upto 30000 K", Avco Corp., TR AD-TM-63-7, March 1963.
66. Yee, H.C., "A Class of High Resolution Explicit and Implicit Shock Capturing Methods", NASA TM 101088, Feb. 1989.
67. Zhong, X., High-Order Finite-Difference Schemes for Numerical Simulation of Hypersonic Boundary-Layer Transition. Journal of Computational Physics, 144, 662-709 (1998).
68. Zhong, X. 1997*a* Direct numerical simulation of hypersonic boundary-layer transition over blunt leading edges. Part II: Receptivity to sound. AIAA Paper 97-0756.
69. Zhong, X. 1997*b* Direct numerical simulation of hypersonic boundary-layer transition over blunt leading edges, Part I: New numerical methods and validation. 35th AIAA - Aerospace Sciences Meeting and Exhibit, January 6–9, Reno, Nevada. AIAA Paper 97-0755.